PERGAMON

International Journal of Heat and Mass Transfer 45 (2002) 2159–2168

International Journal of HEAT and MASS TRANSFER

www.elsevier.com/locate/ijhmt

Analysis of conduction–radiation problem in absorbing, emitting and anisotropically scattering media using the collapsed dimension method

Prabal Talukdar, Subhash C. Mishra *

Department of Mechanical Engineering, Indian Institute of Technology, Guwahati 781 039, India

Received 11 September 1999; received in revised form 26 April 2001

Abstract

Combined conduction–radiation problem is solved using the collapsed dimension method. One-dimensional gray planar absorbing, emitting and anisotropically scattering medium is considered. Non-dimensional medium temperature and heat flux distributions are found for various values of boundary temperature, optical thickness, boundary emissivity and conduction–radiation parameter. Effects of scattering albedo and anisotropy factor are also discussed. For comparison, problems considered are also analyzed with the discrete transfer method and the exact method. Collapsed dimension method is found to give excellent comparison for various radiative parameters considered.

1. Introduction

Over past three decades, considerable attention has been given to the problems associated with combined conduction and radiation heat transfer in participating medium. Some practical applications for such problems include the study of heat transfer in furnaces, IC engines, gas turbine combustors, porous materials, fibrous and foam insulations, manufacturing of glass, fire protection, and so on.

First successful treatment to conjugate conduction–radiation problem in one-dimensional planar medium is attributed to Viskanta and Grosh [1,2]. Subsequently, Viskanta [3] analyzed the effect of scattering albedo on conjugate mode heat transfer. The effect of anisotropy factor was introduced by Yuen and Wong [4] in their analytical formulation of combined conduction–radiation problem in one-dimensional planar medium. All these analytic treatments had been for one-dimensional cases. Owing to difficulties in implementing analytic formulations to conjugate mode problems in multi-dimensional enclosures, in the past decades, a variety of radiation models such as Monte Carlo method (MCM), zone method, discrete ordinate method (DOM), discrete transfer method (DTM), discretized intensity method, finite volume method (FVM), product integration method, etc. have come up. These methods have been attempted by various investigators for combined conduction–radiation problems in one-dimensional Cartesian geometry [5–10]. However, each of these methods has its own merits and demerits [11,12] and, therefore, search for an efficient radiation model still exists.

Major problems with most of the methods have been to:

1. have limited applicability in solving only the radiative part of the problem,
2. problem in coupling the radiative part of the problem to the conductive and/or convective parts, and
3. excessive computational time.

For example, MCM works very well for the radiative part of the problem, but has difficulty in treating the conjugate radiation, conduction and/or convection problems [11,12]. Zone method too handles radiative part very well but faces problem in conjugate modes [11]. Other methods such as DOM, *P–N* approximation, which can handle the conjugate problems, suffer from some other limitations.

* Corresponding author. Tel.: +91-361-690-321; fax: +91-361-690-762.

E-mail address: scm_iitg@yahoo.com (S.C. Mishra).

0017-9310/02/$ - see front matter
PII: S0017-9310(01)00305-2

Nomenclature

a_1	anisotropy factor
G	incident radiant energy in DTM formulation
G'	effective incident radiant energy in CDM formulation
I	effective intensity in CDM formulation
i	intensity in DTM formulation
j	indices
k	thermal conductivity
N	conduction–radiation parameter
M	total numbers of rays
q	net heat flux
S	source function
T	temperature

Greek symbols

β	extinction coefficient
θ	non-dimensional temperature
η	optical thickness coefficient
τ	optical thickness
α	planar angle appearing in CDM
$\Delta\alpha$	angular thickness of the discrete plane
Ψ	non-dimensional heat flux
ω	scattering albedo
σ	Stefan–Boltzmann constant
γ	polar angle in DTM
ϕ	azimuthal angle in DTM
ϵ	emissivity

Subscript

av	average
b	blackbody
C	conductive
L	length
n	nth ray
N	north
R	radiative
S	south
T	total

Superscript

$*$	non-dimensional quantities

In the present work, the collapsed dimension method (CDM) [13–15] is applied for the first time to the conjugate conduction–radiation problem in one-dimensional absorbing, emitting and anisotropically scattering planar medium. CDM is the latest of all the methods and is free from most of the limitations faced by other methods. In this method, three-dimensional radiative information is collapsed to the two-dimensional solution plane in terms of effective intensity and optical thickness coefficient. As all radiative information are collapsed to the two-dimensional solution plane, the form of the governing equations in CDM is completely different than that of the rest of the methods. Complete description of the methods is available in [14].

2. Formulation

Consideration is given to a one-dimensional gray planar medium. South and the north boundaries of the medium are at arbitrary temperatures T_S and T_N, respectively. The medium is absorbing, emitting and anisotropically scattering. Thermal conductivity of the medium is k and is assumed constant. Extinction coefficient β of the medium is also assumed constant.

In absence of convection and heat generation, equation for conservation of total energy in non-dimensional form is written as

$$\frac{d^2\theta}{d\tau^2} = \frac{1}{4N}\frac{d\Psi_R}{d\tau}, \tag{1}$$

where θ is the non-dimensional medium temperature. Here for non-dimensionalization of temperature, south boundary temperature T_S has been taken as reference. Ψ_R is the non-dimensional radiative heat flux and N is the conduction–radiation parameter defined as

$$N = \frac{k\beta}{4\sigma T_S^3}$$

For the problem considered, non-dimensional boundary temperatures are given by

$$\theta(0) = \theta_S = 1, \quad \theta(\tau_L) = \theta_N. \tag{2}$$

2.1. CDM Formulation

Right-hand side of Eq. (1) contains divergence of radiative heat flux $d\Psi_R/d\tau$, which in CDM is given as [14]

$$\frac{d\Psi_R}{d\tau} = \eta(1-\omega)\left[\pi\theta^4 - \frac{G'^*}{2}\right]. \tag{3}$$

In Eq. (3), η is the optical thickness coefficient (OTC), ω is the scattering albedo and G'^* is the non-dimensional effective incident radiation. In CDM, G'^* is given by [14]

$$G'^* = \frac{G'}{\frac{\sigma T_S^4}{2}} = \int_0^{2\pi} I^*(\alpha)\,d\alpha, \tag{4}$$

where I^* is the non-dimensional effective intensity (EI) defined as

$$I^* = \frac{I}{\frac{\sigma T_S^4}{2}} \tag{5}$$

and α is the angle of the EI measured from the control surface. In Eq. (4), EI at any point $n+1$ in the direction α is given by [14]

$$I^*_{n+1} = I^*_n \exp(-\tau\eta) + S^{'^*}[1 - \exp(-\tau\eta)]. \tag{6}$$

This definition of I^* is based on the fact that the optical distance between points n and $n+1$ along the ray direction α is small enough and the source function given by the following equation can be assumed constant over the path-leg. This constant value of the source function is equal to its average values at points n and $n+1$.

$$S^{'^*} = (1-\omega)\theta^4 + \frac{\omega}{2\pi}\left[G^{'^*} + 2a_1 \sin\alpha\, \Psi_R(\tau)\right]. \tag{7}$$

It should be noted that the expression of the source function given by Eq. (7) in terms of effective incident radiation $G^{'^*}$ and radiative heat flux $\Psi_R(\tau)$ results from approximating anisotropic phase function by linear phase function [14,15]

$$p(\alpha' \to \alpha) = 1 + a_1 \sin\alpha \sin\alpha'.$$

In the above equations, a_1 is the anisotropy factor and its values fall in the range $-1 \leqslant a_1 \leqslant +1$. For the case of isotropic scattering, $a_1 = 0$. In CDM, to find out non-dimensional net radiative heat flux Ψ_R appearing in Eq. (7), heat flux is first found due to EIs spanned over a semi-circle, $0 \leqslant \alpha \leqslant \pi$. Then radiative heat flux due to EIs spanned over other half, i.e., $\pi \leqslant \alpha \leqslant 2\pi$ has to be found and vector sum of the two be taken. Heat flux due to EIs spanned over $0 \leqslant \alpha \leqslant \pi$ is given by [14]

$$\Psi_R = \frac{1}{2}\int_{\alpha=0}^{\pi} I^*(\alpha)\sin\alpha\, d\alpha. \tag{8}$$

For evaluation of $G^{'^*}$ and Ψ_R, Eqs. (4) and (8) are numerically integrated as

$$G^{'^*} = \int_0^{2\pi} I^*(\alpha)\, d\alpha = \sum_{n=1}^{2M} I^*(\alpha_n)\Delta\alpha_n, \tag{9}$$

$$\Psi_R = \frac{1}{2}\int_0^{\pi} I^*(\alpha)\sin\alpha\, d\alpha = \frac{1}{2}\sum_{n=1}^{M} c_n I^*(\alpha_n), \tag{10}$$

where in general

$$c_n = \left|\cos\left(\alpha_n + \frac{\Delta\alpha_n}{2}\right) - \cos\left(\alpha_n - \frac{\Delta\alpha_n}{2}\right)\right|. \tag{11}$$

In Eq. (10), M is the number of EIs spanned over $0 \leqslant \alpha \leqslant \pi$ and in Eq. (11), $\Delta\alpha_n$ is the discrete angle in the solution plane over which nth EI is assumed constant. In the present case, $\Delta\alpha_n$ is same for all EIs. To solve energy equation (1), the divergence of radiative heat flux given by Eq. (3) is substituted in Eq. (1). This yields the desired governing integro-differential equation to be solved in CDM

$$\frac{d^2\theta}{d\tau^2} = \frac{1}{4N}\eta(1-\omega)\left[\pi\theta^4 - \frac{G^{'^*}}{2}\right]. \tag{12}$$

It should be noted that Eq. (12) is subjected to the boundary conditions given by Eq. (2).

2.2. DTM Formulation

In DTM, divergence of radiative heat flux $d\Psi_R/d\tau$ appearing in Eq. (1) is given by [16]

$$\frac{d\Psi_R}{d\tau} = 4(1-\omega)\left[\theta^4 - \frac{G^*}{4\pi}\right], \tag{13}$$

where G^* is the non-dimensional incident radiation defined in DTM. If radiation is assumed azimuthally symmetric, which is always true for a planar geometry, G^* is given by [16]

$$G^* = \frac{G}{\frac{\sigma T_S^4}{\pi}} = 2\pi\int_{\gamma=0}^{\pi} i^*(\gamma)\sin\gamma\, d\gamma, \tag{14}$$

where i^* is the non-dimensional intensity and γ is the polar angle. At this point it is worth noting that in DTM, like other methods such as DOM, FVM, etc., intensity $i^*(\gamma,\phi)$ is considered in three-dimensional space. However, in CDM, we deal with EI $I^*(\alpha)$ which is defined only in the two-dimensional solution plane. Because in CDM, all radiative phenomena are first collapsed in the two-dimensional solution plane, expressions for all radiative terms like intensity, heat flux, incident radiation, divergence of radiative heat flux, etc. are different than the corresponding terms in other radiation models. Further, for comparison purpose, only the ultimate radiative quantities like temperature and heat flux calculated from CDM can be compared with other methods. In CDM, the assumption of azimuthally symmetric radiation is not at all required at any stage in the formulation.

With similar arguments as given for CDM, intensity at any point $n+1$ in the ray direction γ is written as [16]

$$i^*_{n+1} = i^*_n \exp(-\tau) + S^*[1 - \exp(-\tau)], \tag{15}$$

where in the above equation, intensity has been normalized as

$$i^* = \frac{i}{\frac{\sigma T_S^4}{\pi}}.$$

In DTM, linear anisotropic phase function is given by

$$p(\gamma' \to \gamma) = 1 + a_1 \cos\gamma \cos\gamma'.$$

For this situation, source function, appearing in Eq. (15), in terms of G^* and Ψ_R is given by

$$S^* = (1-\omega)\theta^4 + \frac{\omega}{4\pi}[G^* + a_1\pi\cos\gamma\ \Psi_R(\tau)]. \quad (16)$$

It should be noted that the meanings of angle γ appearing in DTM and angle α in CDM are different. In CDM, angle α is defined in the two-dimensional solution plane and is measured from the surface. It varies in the range $0 \leqslant \alpha \leqslant 2\pi$. In DTM, γ is the polar angle. It is defined in three-dimensional space and as per convention, it is measured from normal to the surface. For a sphere, it varies from $0 \leqslant \gamma \leqslant \pi$. In DTM, for azimuthally symmetric radiation, non-dimensional net radiative heat flux Ψ_R is given by

$$\Psi_R = 2\int_{\gamma=0}^{\pi} i^*(\gamma)\sin\gamma\cos\gamma\,d\gamma. \quad (17)$$

For numerical evaluation of Eqs. (14) and (17), the entire solid angle is divided into sub-solid angles $\Delta\Omega$ and each sub-solid angle $\Delta\Omega$ is assumed centered around each intensity. The intensity is assumed constant over $\Delta\Omega$. For azimuthally symmetric radiation, i.e., $i(\gamma,\phi) = i(\gamma)$, the entire polar angle ($0 \leqslant \gamma \leqslant \pi$) can be discretized instead of the solid angle. In this situation, G^* and Ψ_R are, respectively, found from

$$G^* = 2\pi\sum_{n=1}^{M} i^*(\gamma_n)\sin\gamma_n\sin\Delta\gamma_n, \quad (18)$$

$$\Psi_R = 2\sum_{n=1}^{M} i^*(\gamma_n)\sin\gamma_n\cos\gamma_n\sin\Delta\gamma_n. \quad (19)$$

To solve energy equation (1), the divergence of radiative heat flux given by Eq. (13) is substituted in Eq. (1) which yields the desired governing integro-differential equation to be solved in DTM

$$\frac{d^2\theta}{d\tau^2} = \frac{1-\omega}{N}\left[\theta^4 - \frac{G^*}{4\pi}\right]. \quad (20)$$

3. Solution procedure

As the solution procedure of the energy equation (1) is same in CDM and DTM, the same is discussed herein with reference to CDM only. To solve Eq. (12), it is expressed in finite difference form as

$$\frac{\theta_{j-1} - 2\theta_j + \theta_{j+1}}{\Delta\tau^2} = \frac{1}{4N}\eta(1-\omega)\left[\pi\theta_j^4 - \frac{G_j^*}{2}\right]. \quad (21)$$

Depending upon the values of conduction–radiation parameter N, solution of Eq. (21) proceeds in two ways. For $N \geqslant 0.01$, first a linear temperature profile is guessed for the right-hand side of Eq. (21). With this guess value of θ, incident radiation G^* is calculated. For evaluation of G^*, EIs I^* are found from Eq. (6). The calculation of intensity starts from the bounding wall. To find out intensity values next to the bounding wall where $n+1$ in Eq. (6) is 1, intensity values at the bounding wall are required. For a gray boundary having emissivity ϵ_w and temperature T_w, boundary intensity in CDM is found from [14]

$$I_0^* = \frac{\epsilon_w T_w^4}{T_S^4} + \frac{1-\epsilon_w}{2}\int_{\alpha=0}^{\pi} I^{*^-}(\alpha)\sin\alpha\,d\alpha. \quad (22)$$

In Eq. (22), I^{*^-} are EIs incident at the point of interest on the concerned boundary from which the boundary intensities are to be found. First term on right-hand side of Eq. (22) is the emitted component whereas the second term represents the reflected component of intensity. If $\epsilon_S = \epsilon_N = 1$, the bounding intensities from the south and the north boundaries are 1 and θ_N^4, respectively. In case of DTM, corresponding form of Eq. (22) is given by

$$i_0^* = \frac{\epsilon_w T_w^4}{T_S^4} + 2(1-\epsilon_w)\int_{\gamma=0}^{\pi/2} i^{*^-}(\gamma)\cos\gamma\sin\gamma\,d\gamma. \quad (23)$$

In CDM, OTC η values for Eqs. (6) and (21) are calculated from the expressions given in [14]. With right-hand side of Eq. (21) known, left-hand side is solved for θ_j using the Thomas algorithm. To get the convergence, under-relaxation is used for small values of N. For values of $N < 0.01$, again a linear temperature profile is guessed as in the first case. However, in this case, left-hand side of Eq. (21) and G^* are calculated simultaneously. Strong under-relaxation is used to get the convergence.

4. Results and discussion

Shown in Figs. 1(a) and (b) are the variations of non-dimensional gas temperature θ with normalized optical depth τ/τ_L. For results presented in the figure, north boundary temperature θ_N is half of that of the south boundary temperature θ_S ($\theta_N = 0.5\theta_S$) and $\epsilon_N = \epsilon_S = 1$. Medium is absorbing–emitting.

In Fig. 1(a), temperature distributions are given for $\tau_L = 1$, whereas in Fig. 1(b), the same are given for $\tau_L = 0.1$. For both values of τ_L, temperature distributions are given for various values of N in the range 0–10. It should be noted that higher values of N signify conduction dominated situation whereas when its value decreases, radiation starts dominating. For $N = 0$, the problem is entirely radiation dominated and the problem becomes the case of radiative equilibrium ($\nabla\cdot\Psi_R = 0$). Above fact is clear from these figures. When values of N are large, temperature profiles are almost linear. As values of N decrease, radiation dominates, temperature profile changes. However, for value of $N = 0$, conduction is absent, gas temperature at the boundaries are not equal to the boundary temperatures.

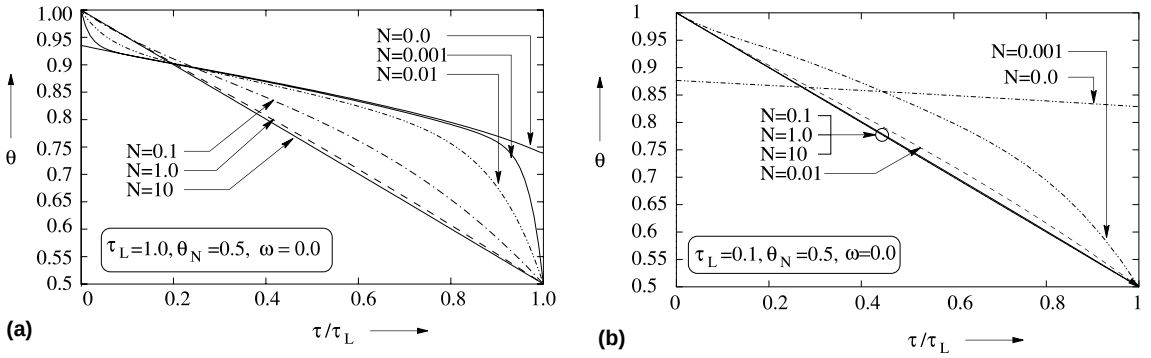

Fig. 1. Effect of conduction–radiation parameter on non-dimensional gas temperature θ.

This phenomena is known as temperature slip and is common for radiative equilibrium problems.

In the present work, it has been found that the number of iterations required for conduction dominated situations is very less compared to radiation dominated cases. For example, for $\tau_L = 1$ and $N \geqslant 1$, convergence is obtained in only 2–3 iterations whereas for $N = 0.1$, 0.01, 0.001 and 0.0001, approximately 80, 120, 600 and 650 iterations are required, respectively. Under relaxation is required for $N \leqslant 0.01$.

In Fig. 2, effect of scattering albedo on temperature distribution is shown. Both boundaries are assumed black. Fig. 2(a) shows the temperature distributions for $N = 0.1$ whereas temperature distributions for $N = 0.01$ are given in Fig. 2(b). Three different values of scattering albedo ($\omega = 0.0$, 0.5 and 1.0) are considered. For these values of ω, temperature distributions are given for two sets of boundary temperatures ($\theta_N = 0.5$ and 0.1). $\omega = 0.0$ represents absorbing–emitting situation whereas for $\omega = 1.0$, medium is purely scattering. Since in the case of $\omega = 1.0$, as seen from energy Eq. (12), temperature profile becomes independent of radiation and hence a linear profile results. Further, as seen from these figures, in radiation dominated situation (for lower values of N), scattering albedo ω has more pronounced effect.

Effect of anisotropy factor a_1 on temperature distribution is shown in Figs. 3(a) and (b). Distributions are given for $\tau_L = 1.0$ and 0.1, conduction–radiation parameter $N = 0.1$ and the north boundary temperature $\theta_N = 0.5$. For scattering situation, scattering albedo ω is taken as 0.5. Results are presented for the two extreme limits of a_1, i.e., $a_1 = +1$ signifying fully forward scattering and $a_1 = -1$ signifying fully backward scattering and isotropic scattering $a_1 = 0$, $\omega = 0.5$. As a reference, temperature distributions for absorbing–emitting situation $\omega = 0$ have also been plotted. It is clear from these figures that for a given value of ω, a_1 has negligible effect on temperature distribution.

Effect of boundary emissivities on temperature distribution is shown in Fig. 4. Emissivity values of both north and south boundaries ϵ_N and ϵ_S are taken to be same ($\epsilon_N = \epsilon_N = \epsilon$). Medium is considered absorbing–emitting, and north boundary temperature $\theta_N = 0.5$. Three different values of emissivity $\epsilon = 0.1$, 0.5 and 1.0 are considered. Effect of boundary emissivity ϵ on θ has been shown for two different values of N (= 0.1 and 0.01). Optical thickness τ_L is 1.0 in both the cases. It is

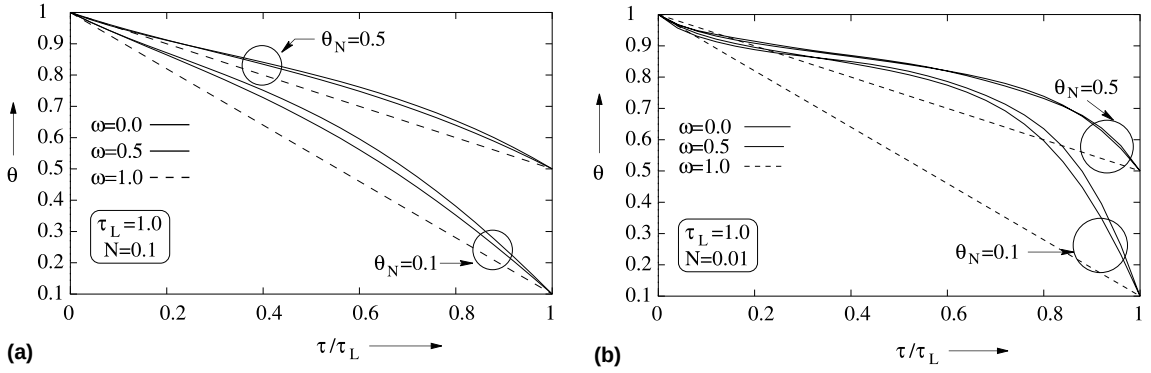

Fig. 2. Effect of scattering albedo ω on non-dimensional gas temperature θ.

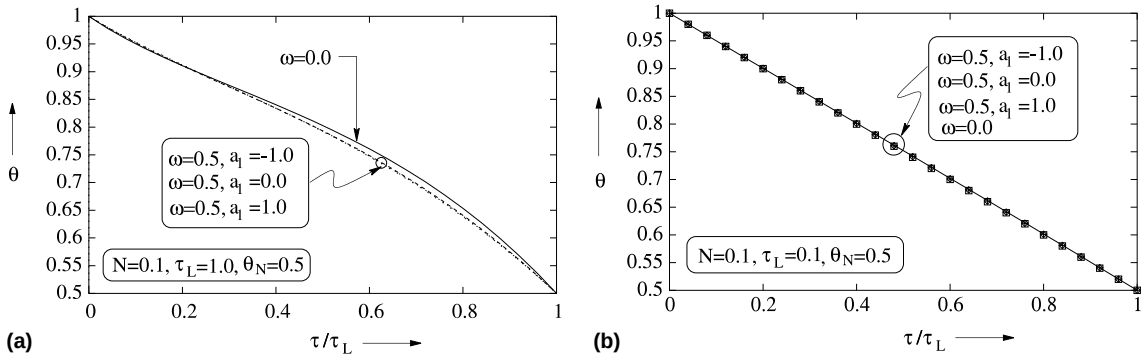

Fig. 3. Effect of anisotropy factor a_1 on non-dimensional gas temperature θ.

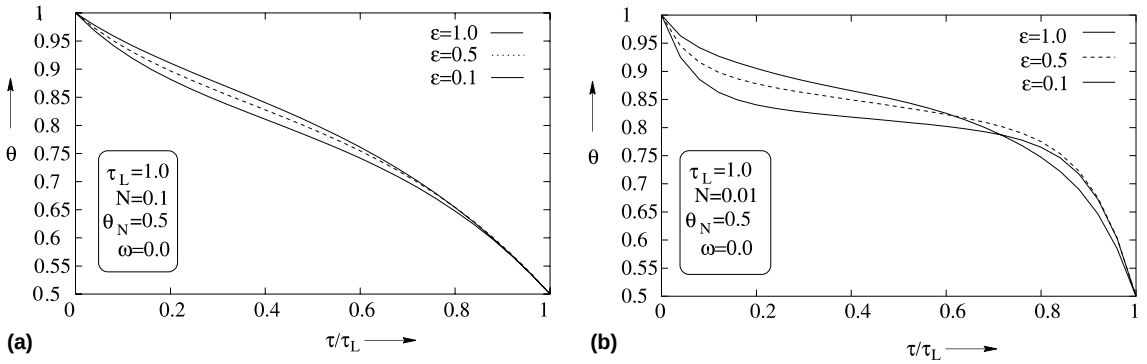

Fig. 4. Effect of wall emissivity ϵ on non-dimensional gas temperature θ; $\epsilon_N = \epsilon_S = \epsilon$.

observed from Figs. 4(a) and (b) that as the boundary emissivities decrease, in other words, as the boundaries become more and more reflecting, variation of θ values for $\epsilon \neq 1$ with respect to θ values for $\epsilon = 1$ increases in the vicinity of the hot (south) boundary. Further, this variation is more for the lower values of N.

In the conduction–radiation problem considered in this work, divergence of total heat flux equals zero, i.e., $\nabla \cdot \Psi_T = 0$, which implies Ψ_T $(= \Psi_C + \Psi_R)$ is constant at all τ/τ_L in the medium. However, conduction heat flux Ψ_C and radiation heat flux Ψ_R will be different at different τ/τ_L in the medium. For given values of N, how conduction and radiation heat fluxes contribute to the total heat flux is depicted in Figs. 5(a)–(f). For this, in all the cases, optical thickness τ_L is taken as 10 and the north boundary temperature $\theta_N = 0.5$. Medium is considered to be absorbing–emitting and the boundaries are taken as black. It is clear from these figures that when N is large, major contribution to Ψ_T comes from conduction. With decrease in its value, contribution from radiation starts increasing. For $N = 0.01$, the total heat flux is primarily due to radiation. Other interesting point to be noted from these figures is that conduction heat flux is always higher at the cold (north) boundary, whereas radiation heat flux is always higher at the hot (south) boundary.

To have some quantitative idea, how CDM results for total heat flux Ψ_T computed using different number of rays compare with DTM results generated by the authors and exact results [1,4], some sample data have been presented in Tables 1–3. In Table 1, results are presented for absorbing–emitting medium confined between black boundaries. Here, comparisons are made for four values of τ_L and two sets of boundary temperatures. For given values of τ_L and boundary temperatures, N values are taken to be 0.0, 0.1, 1.0 and 10. Here, the CDM results for different number of rays are compared with the DTM results for different number of rays and exact results given in [1]. In Table 2, comparisons of CDM results for different number of rays are made with DTM results for different number of rays and exact results [4]. These comparisons are made for three medium conditions, e.g., (a) absorbing–emitting $\omega = 0$, (b) absorbing, emitting and isotropically scattering with $\omega = 0.5$, and (c) absorbing, emitting and anisotropically scattering with $\omega = 0.5$ and $a_1 = -1.0$ and 1.0. For given values of ω and a_1, results are compared for $\tau_L = 1.0$ and $N = 1.0$. Here the boundaries are assumed black. In

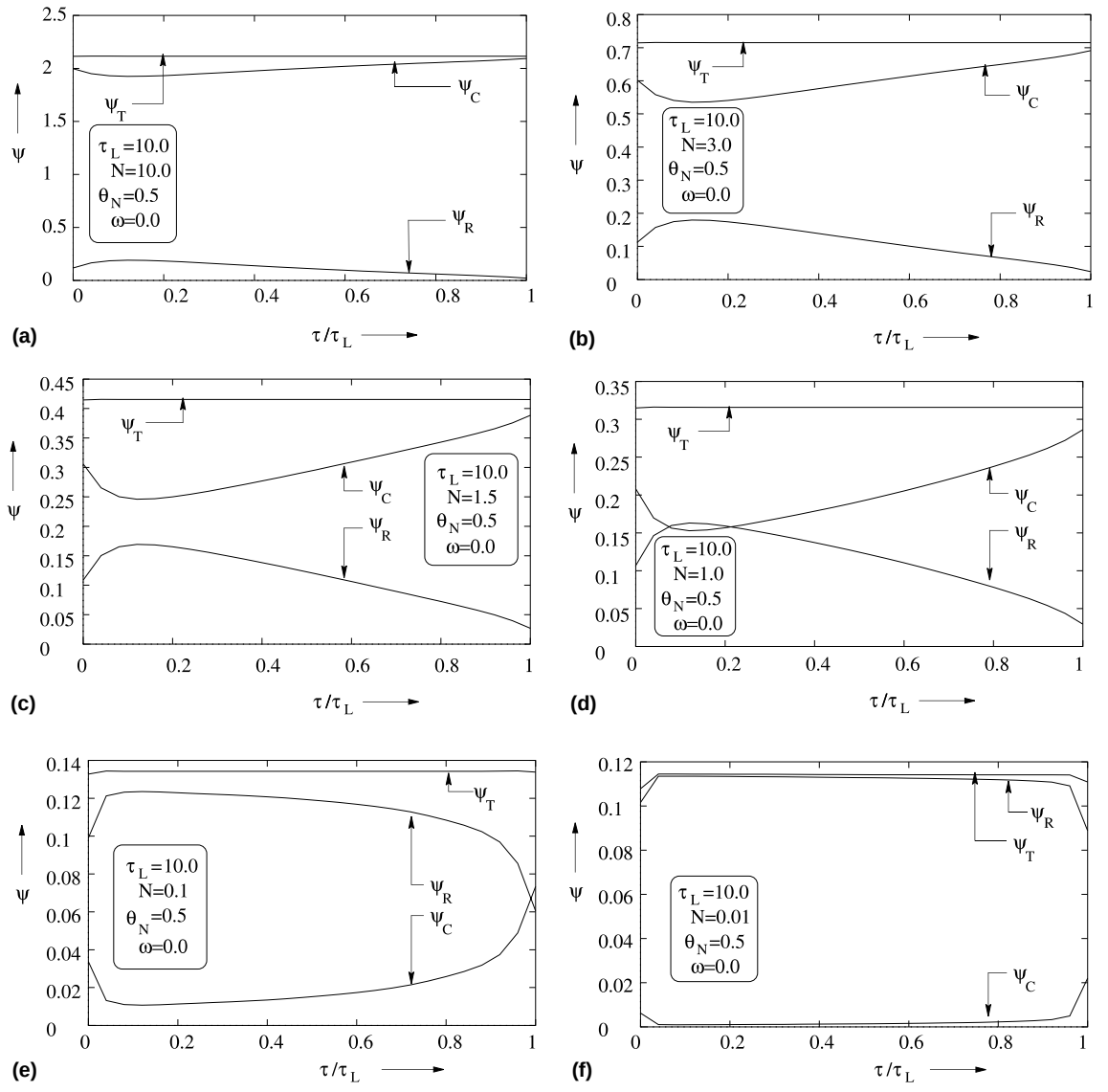

Fig. 5. Variation of non-dimensional conductive heat flux Ψ_C, radiative heat flux Ψ_R and total heat flux Ψ_T with normalized optical depth τ/τ_L for various values of conduction–radiation parameter N.

Table 3, CDM results are compared with [1]. For a given value of τ_L, boundary temperatures and N, emissivity of both the boundaries have been taken to be 0.1. It is observed from these tables that even with less number of rays, CDM yields excellent comparison with other methods. For given τ_L and boundary temperatures θ_N and θ_S, for higher values of N, CDM and DTM require less number of rays to give analytic accuracy, whereas with decrease in values of N, i.e., in radiation dominated situation, CDM yields accurate results with 12–16 rays whereas DTM requires more number of rays.

For a given set of parameters, to have an idea of computational time required by the CDM and the DTM, test runs were taken on HP-9000 computer. For example, for $N = 0.01$, $\omega = 0.0$, $\tau_L = 1.0$, $\theta_N = 0.5$ and $\epsilon_S = \epsilon_N = 1$, for getting the total heat flux Ψ_T within 5% of the exact result, CPU time in CDM has been found to be 2.57 seconds, whereas the same in DTM has been found to be 8.03 seconds. This signifies that CDM is computationally more efficient than the DTM.

For a given enclosure optical thickness τ_L, the effect of conduction–radiation parameter N on total heat flux Ψ_T has been shown in Fig. 6. Results have been presented for $\tau_L = 0.1$ and 1.0. In both the cases, north boundary temperature $\theta_N = 0.5$, medium is absorbing–emitting and boundaries are black. Both DTM and CDM results are

Table 1
Comparison of total heat flux Ψ_T calculated from CDM with DTM and exact results [1]; $\epsilon_S = \epsilon_N = 1.0$, $\omega = 0.0$

τ_L	θ_N	N	Non-dimensional total heat flux, Ψ_T					
			CDM 8 rays	CDM 12 rays	CDM 16 rays	DTM 32 rays	DTM 64 rays	Exact [1]
0.1	0.5	0	0.857	0.857	0.8575	0.8585	0.8587	0.859
		0.01	1.079	1.079	1.079	1.079	1.079	1.074
		0.1	2.879	2.88	2.88	2.879	2.879	2.88
		1.0	20.88	20.88	20.879	20.879	20.88	20.88
		10.0	200.88	200.88	200.88	200.88	200.88	200.88
1.0	0.1	0	0.545	0.550	0.554	0.553	0.554	0.556
		0.01	0.630	0.634	0.636	0.630	0.630	0.658
		0.1	0.968	0.972	0.974	0.968	0.968	0.991
		1.0	4.197	4.201	4.204	4.197	4.198	4.218
		10.0	36.59	36.6	36.6	36.59	36.59	36.6
1.0	0.5	0	0.511	0.516	0.519	0.518	0.519	0.518
		0.01	0.559	0.563	0.572	0.566	0.567	0.596
		0.1	0.768	0.772	0.774	0.768	0.769	0.798
		1.0	2.572	2.575	2.580	2.571	2.572	2.60
		10.0	20.57	20.57	20.58	20.57	20.57	20.60
10.0	0.5	0	0.108	0.108	0.106	0.108	0.107	0.102
		0.01	0.111	0.113	0.114	0.101	0.110	0.114
		0.1	0.130	0.131	0.132	0.134	0.132	0.131
		1.0	0.312	0.313	0.314	0.315	0.315	0.315
		10.0	2.112	2.113	2.114	2.114	2.114	2.114

Table 2
Comparison of heat flux result Ψ_T calculated from CDM with DTM and exact results [4]; $\epsilon_S = \epsilon_N = 1.0$

N	ω	a_1	Non-dimensional total heat flux, Ψ_T for $\tau_L = 1$				
			CDM 16 rays	CDM 64 rays	DTM 16 rays	DTM 64 rays	Exact [4]
1.0	0	0	2.575	2.579	2.572	2.572	2.60
	0.5	0	2.544	2.546	2.548	2.55	2.55
	0.5	1.0	2.564	2.565	2.585	2.594	2.594
	0.5	−1.0	2.490	2.492	2.510	2.512	2.512

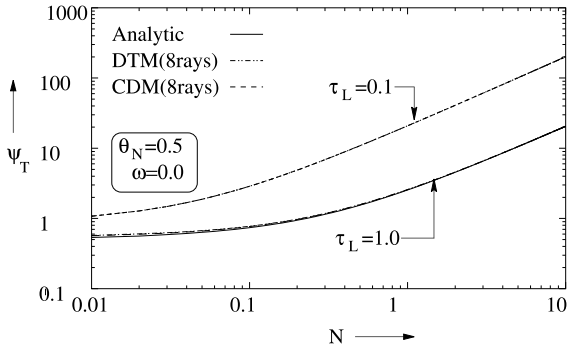

Fig. 6. Variation of total heat flux Ψ_T with conduction–radiation parameter N.

compared with exact results generated by the authors. CDM results with 8 rays are found in very good agreement with the DTM results with 8 rays and exact results.

To show the effect of conduction–radiation parameter N on the values of conductive heat flux Ψ_C, radiative heat flux Ψ_R and the total heat flux Ψ_T at the two boundaries, results have been presented in Fig. 7. In Figs. 7(a) and (b), these results are presented for $\tau_L = 0.1$ and 1.0, respectively. In both the cases, north boundary temperature is half of that of the south boundary temperature $\theta_N = 0.5$. These effects are checked for $\omega = 0.0$, 0.5 and 0.9. In these figures, suffix (N and S) over respective heat flux represents heat flux over a particular boundary. For example, Ψ_{CN} represents conductive heat flux Ψ_C over north boundary. One interesting point to be noted from these plots is that it is

Table 3
Comparison of heat flux Ψ_T calculated from CDM with exact results [1]; $\epsilon_S = \epsilon_N = 0.1$

τ_L	θ_N	N	Non-dimensional total heat flux, Ψ_T			
			CDM 8 rays	CDM 16 rays	CDM 32 rays	Exact [1]
0.1	0.5	0	0.494	0.494	0.494	0.49
		0.01	0.276	0.277	0.276	0.267
		0.1	2.077	2.077	2.077	2.078
		1.0	20.07	20.07	20.07	20.08
		10.0	200.07	200.07	200.07	200.08
1.0	0.1	0	0.510	0.511	0.511	0.51
		0.01	0.196	0.196	0.196	0.22
		0.1	0.567	0.568	0.570	0.591
		1.0	3.812	3.811	3.810	3.752
		10.0	36.21	36.21	36.21	36.22
1.0	0.5	0	0.0479	0.0479	0.0479	0.047
		0.01	0.155	0.155	0.155	0.156
		0.1	0.403	0.401	0.400	0.393
		1.0	2.220	2.220	2.223	2.245
		10.0	20.22	20.22	20.22	20.25
10.0	0.5	0	0.039	0.039	0.0387	0.036
		0.01	0.086	0.087	0.088	0.090
		0.1	0.112	0.113	0.113	0.115
		1.0	0.304	0.302	0.302	0.297
		10.0	2.104	2.105	2.106	2.107

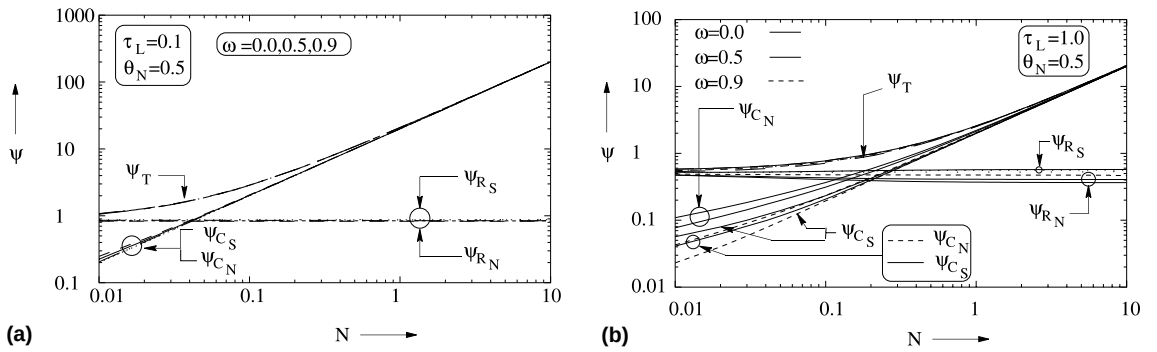

Fig. 7. Effect of conduction–radiation parameter N on non-dimensional conductive, radiative and total heat fluxes at the boundaries.

mainly the conductive heat flux Ψ_C at the boundary that keeps on increasing with conduction–radiation parameter N. There is not much variation in the radiative heat flux Ψ_R at the boundary. For $\tau_L = 0.1$, on both the boundaries, Ψ_R is constant. For $\tau_L = 1.0$, Ψ_R is different at the two boundaries and this difference decreases with decrease in N. For the limiting case, $N = 0$, the problem changes to radiative equilibrium case, Ψ_R is same at the two boundaries. Further it is observed that when problem is highly conduction dominated ($N \to \infty$), Ψ_C is same at the two boundaries. With decrease in the values of N, i.e, as radiation starts dominating, difference between the Ψ_C values at the two boundaries increases. For a given value of ω, Ψ_C is lower at the south boundary. Further it can be observed from these results that ω has more pronounced effect on Ψ_C than on Ψ_R. Effect of ω on Ψ_C decreases with increase in N.

5. Conclusions

Combined conduction–radiation problem in one-dimensional gray planar absorbing, emitting and anisotropically scattering medium has been investigated by the CDM. Like DOM, DTM and FVM, CDM code for radiative problems has been found compatible with conduction code. Temperature distributions have been found for various values of optical thickness τ_L, conduction–radiation parameter N, boundary emissivity ϵ, scattering albedo ω, anisotropy factor a_1 and boundary

temperatures. CDM has been found to correctly predict temperature and heat flux information. Relative contributions of conduction heat flux Ψ_C and radiation heat flux Ψ_R to the total heat flux Ψ_T have also been presented for various values of N and τ_L. These results very correctly show how relative contributions of each mode vary. For comparison purpose, for some test cases, results for heat flux have also been generated by the DTM and both these results have been compared with exact results presented in the literature. CDM results have been found in very good agreement with other methods. Although, in conduction dominated situation, both CDM and DTM have been found to take approximately same amount of computational time, in radiation dominated situation, CDM has been found much more economical than the DTM.

References

[1] R. Viskanta, R.J. Grosh, Heat transfer by simultaneous conduction and radiation in an absorbing medium, ASME J. Heat Transfer 84 (1962) 63–72.

[2] R. Viskanta, R.J. Grosh, Effect of surface emissivity on heat transfer by simultaneous conduction and radiation, Int. J. Heat Mass Transfer 5 (1962) 729–734.

[3] R. Viskanta, Heat transfer by conduction and radiation in absorbing and scattering materials, ASME J. Heat Transfer 87 (1965) 143–150.

[4] W.W. Yuen, L.W. Wong, Heat transfer by conduction and radiation in a one-dimensional absorbing emitting and anisotropically-scattering medium, ASME J. Heat Transfer 102 (1980) 303–307.

[5] A.C. Ratzell III, J.R. Howell, Heat transfer by conduction and radiation in one-dimensional planar medium using differential approximation, ASME J. Heat Transfer 104 (1982) 388–399.

[6] R. Fernandes, J. Francis, J.N. Reddy, A finite-element approach to combined conductive and radiative heat transfer in a planar medium, in: Heat Transfer and Thermal Control, Progress in Aeronautics and Astronautics, vol. 78, AIAA, New York, 1981, pp. 92–109.

[7] M. Miskin, G.J. Kowalski, Application of Monte Carlo technique to the steady state radiative and conductive heat transfer through a participating medium, ASME Paper No. 83-WA/HT-27, 1983.

[8] C.H. Ho, M.N. Özişik, Simultaneous conduction and radiation in a two-layer planar medium, J. Thermophys. Heat Transfer 1 (2) (1987) 154–161.

[9] W.W. Yuen, M. Khatami, Transient radiative heating of an absorbing emitting and scattering material, J. Thermophys. Heat Transfer 4 (2) (1990) 193–198.

[10] R. Siegel, Finite difference solution for transient cooling of a radiating–conducting semitransparent layer, J. Thermophys. Heat Transfer 6 (1) (1992) 77–83.

[11] J.R. Howell, Thermal radiation in participating media: The past, the present and some possible future, ASME J. Heat Transfer 110 (1988) 1220–1229.

[12] S.C. Mishra, M. Prasad, Radiative heat transfer in participating media – a review, Sádhana 23 (Part 2) (1998) 213–232.

[13] D.A. Blank, S.C. Mishra, Use of 2-D the collapsed dimension method in gray enclosures with absorbing–emitting–isotropic scattering media in radiative equilibrium, Numer. Heat Transfer: Part B 30 (4) (1996) 469–481.

[14] S.C. Mishra, A novel computational approach for the solution of radiative heat transfer problems in participating media, PhD Thesis, IIT, Kanpur, India, 1997.

[15] S.C. Mishra, M. Prasad, Radiative heat transfer in absorbing–emitting–scattering gray media inside 1-D Cartesian enclosure using the collapsed dimension method, Int. J. Heat Mass Transfer 45 (3) (2001) 697–700.

[16] N.G. Shah, New method of computation of radiation heat transfer combustion chambers, PhD Thesis, Imperial College, University of London, England, 1979.